ROSTISLAV DUDA

QUANTUM TRANSPORT THROUGH TWO-DIMENSIONAL NANOCAVITIES

Bachelor of Science thesis

Examiners:
Joonas Keski-Rahkonen and Esa Räsänen

ABSTRACT

ROSTISLAV DUDA: Quantum transport through two-dimensional nanocavities
Tampere University
Bachelor of Science Thesis, 24 pages
January 2019
Bachelor's Degree Programme in Science and Engineering
Major: Physics
Examiners:
Joonas Keski-Rahkonen and Esa Räsänen

Keywords: thesis, computational physics, quantum transport

In this thesis work, we present a highly-optimized numerical simulation framework for performing transport calculations in a non-interacting equilibrium. The algorithm has been designed in accordance with the Landauer-Büttiker approach to quantum transport. We outline the algorithm and demonstrate its flexibility and versatility in three different transport scenarios: a single state molecular junction, a two-state molecular junction and a nanocavity with a potential barrier. We study transmission, conductance, and current flowing through these systems. The behavior of the numerical results of the transport simulations has been found to be in good agreement with the theory. We motivate the usage of the algorithm implemented in the TINIE software package in the context of quantum scarring phenomena and non-zero uniform magnetic fields.

PREFACE

First, I would like to thank my family and friends for continuously encouraging me in the process of writing this thesis. I am also grateful to Joonas Keski-Rahkonen and Janne Solanpää for directing my research work. TINIE would never see the light of day without their wise and thorough guidance. Finally, I would like to thank Esa Räsänen for giving me an opportunity to work in the Quantum Control and Dynamics Group for the last two years. The experience I have received as a research assistant has most definitely proven to be invaluable.

In Tampere, Finland, on 26 November 2018

Rostislav Duda

CONTENTS

1. INTRODUCTION

The pursuit of empirical truth by means of scientific research and investigation has always been one of the most fruitful and insightful endeavors of mankind. Advancements in science lead to the creation of new technology. New technology facilitates everyday tasks and routines, leading to societal changes. Most importantly, scientific knowledge reshapes the way we think about the world and reality on both the largest and the smallest of scales. In that respect, the past century has provided us with new revelations and paradigm shifts. For instance, the twentieth-century developments in quantum theory shattered the deterministic approach to physics that was dominant in the past. Quantum physics describes the universe and its constituents in terms of wave functions: entities that give the probability of some event happening, but never guarantee its measurable occurrence. Indeterminism is an inherent feature of this theory.

Quantum mechanics allows for some effects that would otherwise be considered impossible in classical physics. For example, there is a possibility of an electron *tunneling* through a barrier that it would normally be unable to surpass. The idea of quantum tunneling will be crucial in this thesis. One of the main reasons why quantum effects have not been observed until the preceding century was due to the fact that they only reveal themselves on the nanometer scale and below. On the macroscale the world can be treated as approximately classical.

Quantum theory is nowadays more crucial to advancements in various fields of technology than ever before. Of particular interest to us is its contribution to the integrated circuit industry. Computers are made of integrated circuits, which are in turn made of transistors that act as the ”tracks”, through which the electrons in the computer flow, carrying binary data. The exponentially increasing computational power of the subsequent generations of computing machines has been governed by Moore’s law ever since the 1960s. According to Moore’s law, the amount of transistors in a dense integrated circuit doubles every two years [1]. However, now there is a need for a revolution in the field of computing.

As the transistor sizes now approach only a few nanometers, the behavior of electrons in a transistor can no longer be thought of as classical. Hence, we are tasked with incorporating the quantum mechanical properties of the electron in the field of transistor manufacture. Transistors are the fundamental building blocks of modern computers. Thus, the development of the nanoscale transistor technology and its subsequent use in the integrated circuit industry have led to the emergence of *quantum computing*.

As mentioned above, electrons confined to a small region of space, such as a nanoscale transistor, have a probability to tunnel outside of the system. Our task in designing quantum

transistors is to find a way to maximize the probability of an electron going from one system to another and not tunneling in unwanted regions leading to loss of fidelity. We thus turn our attention to the field of *quantum transport* that studies the formation of current in nanoscale systems. Studies on the transport properties of nanoscale transistors or nanocavities in general can provide us with insights into the ways the electron flow may be controlled at the smallest scale. Such knowledge is crucial in the development of nanotechnology.

In this thesis we investigate electron transport in two-dimensional systems utilizing a numerical transport simulation software package TINIE, that has been developed throughout the course of this study. In particular, we intend to demonstrate TINIE's functionality, as well as the potential it has as a transport code to simulate quantum dynamics. Chapter 2 outlines the essential theory behind quantum transport phenomena, the typical structure of a transport experiment, and the Landauer-Büttiker approach to quantum transport. Chapter 3 goes into the details of TINIE's main algorithm and features, as well as the description of the systems to be numerically simulated. Chapter 4 presents the results and analysis of the performed numerical simulations. The thesis is then concluded in Chapter 5.

2. THEORETICAL BACKGROUND

We begin by making a distinction between transport phenomena in nanoscale systems and transport in mesoscopic or microscopic systems. The fundamental difference is that nanoscale transport is based on quantum physics [2]. Additionally, as we are concerned entirely with the behavior of electrons in the nanocavity, we restrict the scope of our problem to the study of electron transport. In quantum mechanics, electrons are described by wave functions $\psi(\mathbf{r}, t)$. The current is mathematically described by means of an operator $\hat{I}$ that acts on the wave function.

Wave functions have the property called *phase*. An interaction between waves with different phases leads to a process of interference, which can be either constructive or destructive. When studying transport systems with real-life applications, normally we are interested in the *coherent transport*: transport processes that do not alter the phase of the charge carriers [3].

The field of transport is rich in different theories describing transport phenomena from various perspectives. However, they can be grouped into two main approaches:

1. The electrical current is a consequence of an applied electric field: *the field is the cause and the current is a response to this field*. Drude conductivity model [4], Kubo formalism [5] and the Boltzmann equation [6] are the key theories in this approach.
2. The electric field is a consequence of the charge carrier pileup on the surface of the conductor induced by the carrier flow through that surface: *the current is the cause and the field is a response to current*. This approach is usually referred to as the Landauer-Büttiker formalism [7].

In order to proceed in our investigation of transport phenomena, we must first choose which of the two approaches to use, since both describe the same physical phenomena, but from different standpoints. We will be using the *Landauer-Büttiker approach* for the rest of this thesis work. Sec. 2.3 will discuss the theory behind it, as well as the underlying assumptions.

To summarize, we have so far made the following assumptions regarding the transport process to narrow the scope of our problem:

1. The charge carriers are electrons exclusively;
2. The transport system is on a nanoscopic scale;
3. The transport process in the system is coherent;
4. The transport process in the system is described by the Landauer-Büttiker formalism.

2.1 Structure of a transport experiment

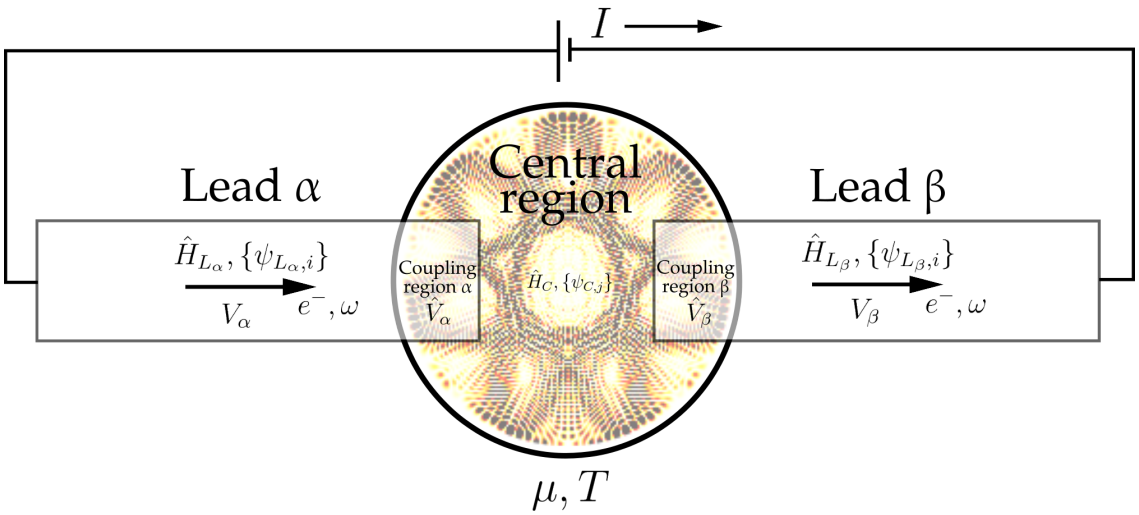

Figure 2.1. *Typical two lead transport system of temperature T with chemical potential μ. Leads have different bias potentials V_α and V_β, leading to emergence of current I. We examine the behavior of current with varying energy ω of the probe electrons. In the center we see a typical probability density function corresponding to one of the central region eigenstates.*

A typical electronic transport experiment in a semiconductor system consists of a two-dimensional electron gas (2DEG) confined to a small *nanocavity* region by an external potential and two or more charge *reservoir* regions that can supply and receive an arbitrary amount of carriers without changing its internal state.

We may interpret this as follows: the nanocavity is constantly supplied by a flux of electrons through the reservoirs that act as leads connected (or coupled) to the ends of the cavity. There are many various conventions regarding the naming of the nanocavity region e.g., quantum dot, device, central region. These terms are interchangeable, so for the sake of convention, from now on we will refer to the nanocavity region as the *central region* or *center*. Similarly, reservoir regions have many names e.g., leads or electrodes. In this thesis, they are referred as the *lead regions* or *leads*.

The current can be generated by introducing a bias voltage into one of the leads. This results in a non-zero potential energy difference between the two (or more) leads, leading to the formation of current. Under specific assumptions that are outlined in Sec. 2.3, this bias can be interpreted as the *electrochemical potential difference* μ between the leads [2]. We can then experiment with this system by letting electrons with a specific *probe energy* ω flow through the center.

By varying the probe energy, we can examine the dependence of the transport properties on the energy of incoming electrons. In particular, we are interested in transmission and current. The *transmission* is defined as the probability of an electron with specific probe energy to move from one lead, through the center, and into another lead. The *current* is

defined as the rate of charge flow from one lead to another. Figure 2.1 illustrates a typical set-up of a transport experiment with two reservoirs.

2.2 Quantum mechanical description

Before describing the Landauer-Büttiker approach, we shall first outline the mathematical description of the central region, the lead regions and the region where they overlap, which is called the *coupling region*. We start by considering *closed systems* that do not interact with their surroundings. Any closed quantum mechanical system at any given point can be described by the Schrödinger equation:

$$\hat{H}\psi_i(\mathbf{r}) = E_i\psi_i(\mathbf{r}), \tag{2.1}$$

where $\hat{H}$ is the *Hamiltonian* of the system and E_i is the energy corresponding to the state $\psi_i(\mathbf{r})$. An arbitrary state of the system can then be described in terms of this set:

$$\psi(\mathbf{r}) = \sum_i c_i\psi_i(\mathbf{r}), \tag{2.2}$$

where c_i are arbitrary complex number coefficients such that $|c_i|^2$ corresponds to the probability of the occurrence of state $\psi_i(\mathbf{r})$.

Each lead can be described by its Hamiltonian $\hat{H}_{L_\alpha}$ and the corresponding sets of eigenfunctions $\{\psi_{L_\alpha,i}(\mathbf{r})\}$, where the index L_α corresponds to the lead α. Likewise, we describe the central region by its Hamiltonian $\hat{H}_C$ and its set of eigenfunctions $\{\psi_{C,j}(\mathbf{r})\}$.

To complete our description of the transport system, we need to take into the account the transition of the electron from the reservoir to the center and vice versa. This is accomplished by means of computing the coupling matrices between the lead states and the states of the central region. From now on we adopt the Hartee atomic unit convention. We use the coupling of the form:

$$\left[\hat{V}_\alpha\right]_{ij} = \int_\Omega \mathrm{d}\mathbf{r}\, \psi^*_{L_\alpha,i}(\mathbf{r}) \left[-\frac{1}{2}\nabla^2 + V_{\mathrm{pot}}(\mathbf{r})\right] \psi_{C,j}(\mathbf{r}), \tag{2.3}$$

where $\hat{V}_\alpha$ is the coupling matrix between the lead α and the central region, $V_{\mathrm{pot}}(\mathbf{r})$ is the potential operator describing the central region and Ω is the region where the lead and center overlap.

As a summary, to fully describe a transport system, we need the following:

- Central region described by Hamiltonian $\hat{H}_C$ and wave functions $\{\psi_{C,j}(\mathbf{r})\}$;
- Lead regions described by Hamiltonians $\hat{H}_{L_k}$ and wave functions $\{\psi_{L_k,i}(\mathbf{r})\}$;
- Coupling regions described by coupling matrices $\hat{V}_\alpha$.

2.3 Landauer-Büttiker approach to quantum transport

As mentioned above, the Landauer-Büttiker formalism is based on the idea that the electric field is a consequence of carrier flow. However, this is not the only assumption of the theory. In the theoretical considerations below we follow Refs. [2, 3, 7]. Before we can proceed, we shall outline all the other assumptions:

1. The transport system is an *open* quantum system, i.e., a system where electrons coming into the lead are completely uncorrelated with electrons going out of it. In such a system, the bias energy is the electrochemical potential difference between the leads, as mentioned in Sec. 2.1.
2. The transport system possesses a *unique stationary solution*, i.e., an equilibrium that it will attain after a sufficiently long period of time.
3. The electrons in the transport system obey *scattering boundary conditions*. They are prepared into wave packets far from the quantum dot. These wave packets then move towards the center through the lead regions, scatter in the center and then move far away from it without further scattering.
4. The Hamiltonian of the system can be described by a *single particle* Hamiltonian of the form $\hat{H} = -\frac{1}{2}\nabla^2 + V(\mathbf{r})$.
5. The leads do not interact with each other. This means that the energy filling of a lead is *independent* from energy filling of any other lead in the system. Hence, we can describe the energy distribution in each lead using their local equilibrium Fermi-Dirac distributions.

Finally, the Landauer-Büttiker formalism in its complete form describes *time-dependent non-equilibrium transport* [2]. Before the current reaches a *steady state* (a point where the time average of the current operator $\langle \hat{I} \rangle$ becomes constant), it undergoes a complex process of fluctuation and change, governed by the time-evolution of a *statistical operator* $\hat{\rho}(t)$. We will not examine this complex behaviour. Instead, we assume that we have already reached the steady state after some long period of time, thus dealing with a time-independent *non-interacting equilibrium* transport problem. Now we can describe the mathematics underlying the formalism.

At the core of the Landauer-Büttiker approach is the process of electron scattering. *Scattering* can be defined as the change of the momentum of the electron due to its interaction with the medium in which it propagates. The scattering properties of a transport system can be elegantly described in terms of a scattering matrix, or *S-matrix*. Given a transport system with a total number of states in all the leads equal to N_S, S-matrix $S \in \mathbb{C}^{N_S \times N_S}$ is a matrix such that the electron transmission probability $\mathcal{T}_{ij}$ from state i to a state j is $\mathcal{T}_{ij} = |S_{ij}|^2$. Similarly, to calculate the electron transmission probability $\mathcal{T}_{\alpha\beta}$ from a lead α to a lead β, we sum over all the possible state transitions belonging to these leads [3]:

$$\mathcal{T}_{\alpha\beta} = \sum_{i \in \alpha} \sum_{j \in \beta} \mathcal{T}_{ij}. \tag{2.4}$$

For the sake of convenience, the Latin indices correspond to individual states in the lead, whereas the Greek indices are related to the entire lead. We see that the *transmission matrix* $\mathcal{T} \in \mathbb{R}^{N_L \times N_L}$, where N_L is the total number of leads, is readily obtained from the S-matrix. Furthermore, S is unitary due to the law of conservation of current, which in turn makes $\mathcal{T}$ symmetric [3].

In essence, the S-matrix describes a response in one lead due to an excitation in the other. Naturally, for a more thorough analysis of the transport system we would want to know the response *at any point* $\mathbf{r}$ due to an excitation at any other point $\mathbf{r}'$. Such a generalization of the S-matrix exists in the form of *Green functions* [3]. It is applied in many different contexts in both physics and mathematics, but we will focus on its use in the context of electron transport. We start by noting that Eq. (2.1) can be re-written as

$$\left[E - \hat{H}\right] \psi(\mathbf{r}) = 0, \tag{2.5}$$

where $\hat{H}$ is the total Hamiltonian of the transport system. This Hamiltonian is a linear differential operator due to the single-electron approximation [2]. By the general theory of differential equations this implies that there exists a Green function $\hat{G}(\mathbf{r}, \mathbf{r}')$ such that [3]

$$\left[E - \hat{H}\right] \hat{G}(\mathbf{r}, \mathbf{r}') = \hat{1}\delta(\mathbf{r} - \mathbf{r}'), \tag{2.6}$$

where $\delta(\mathbf{r} - \mathbf{r}')$ is the Dirac delta function and $\hat{1}$ is the identity operator. The Green function in this time-independent case can then be physically interpreted as the wave function at $\mathbf{r}$ due to an impulse excitation originating from $\mathbf{r}'$ [3]. However, when moving towards more abstract eigenfunction bases, this meaning of Green function may be obscure. Since we investigate the transport system by letting probe electrons go through it, energy E will be the energy ω of the probe electron. Hence,

$$\hat{G}(\omega) = \left[\omega - \hat{H}\right]^{-1}. \tag{2.7}$$

The Green function is an inverse of a differential operator, so in order to specify it uniquely, we must specify the boundary conditions [2]. To that end, it is customary to define *advanced* and *retarded* Green functions $\hat{G}^A$ and $\hat{G}^R$. In the real space, the former corresponds to incoming waves that disappear at $\mathbf{r}'$, while the latter corresponds to outgoing waves originating at $\mathbf{r}'$:

$$\hat{G}^R(\omega) = \left[\omega\hat{1} - \hat{H} + \mathrm{i}\eta\hat{1}\right]^{-1} \quad \text{and} \quad \hat{G}^A(\omega) = \left[\omega\hat{1} - \hat{H} - \mathrm{i}\eta\hat{1}\right]^{-1}, \tag{2.8}$$

where η is a positive infinitesimal number that defines the boundary condition. Since $\omega\hat{1}$ and $\hat{H}$ are Hermitian, $\hat{G}^R(\omega) = \left[\hat{G}^A(\omega)\right]^\dagger$.

In all the equations above, $\hat{H}$ is the total Hamiltonian of the transport system. However, in Sec. 2.2, we only mention the Hamiltonians of the individual non-interacting systems. Thus, in order to construct the total Hamiltonian, we also need to account for their interaction. This interaction is described by the *(embedding) self-energy operator*. Scattering from the

lead to the center may occur in an infinite number of ways: electron may freely propagate through the lead into the central region, or it may scatter once during propagation, or twice, etc. All of those possible scattering events for a lead α interacting with the central region can be combined into a quantity called the self-energy operator $\hat{\Sigma}_\alpha(\omega)$, which in a time-independent case is broken down into advanced and retarded components similarly to the Green function [3]:

$$\hat{\Sigma}_\alpha^R(\omega) = \hat{V}_\alpha^\dagger \hat{G}_\alpha^R(\omega)\hat{V}_\alpha \quad \text{and} \quad \hat{\Sigma}_\alpha^A(\omega) = \hat{V}_\alpha^\dagger \hat{G}_\alpha^A(\omega)\hat{V}_\alpha. \tag{2.9}$$

In a manner, analogous to the Green function, it can be shown that $\hat{\Sigma}_\alpha^R(\omega) = \left[\hat{\Sigma}_\alpha^A(\omega)\right]^\dagger$. Once we know the self-energies, we can write the total Hamiltonian of the system as

$$\hat{H} = \hat{H}_C + \sum_\alpha \hat{\Sigma}_\alpha. \tag{2.10}$$

This Hamiltonian allows us to compute the Green functions of the system open to the electron transfer from the leads to the center and vice versa. Hence, we have effectively transformed our closed lead and center regions into an open system!

Eigenenergies of the total Hamiltonian of the system as per Eq. (2.10) may be complex if self-eneries are complex. If the original set of eigenenergies of the center region ϵ_i has been shifted by $\xi_i + \mathrm{i}\zeta_i$, the time dependence of the eigenstate ψ_i of $\hat{H}$ is now of the form [3]

$$\psi_i(t) \sim \exp(-\mathrm{i}(\epsilon_i - \xi_i - \mathrm{i}\zeta_i)t) = \exp(-\mathrm{i}(\epsilon_i - \xi_i)t)\exp(-\zeta_i t). \tag{2.11}$$

We can see that an additional decay term has been introduced into the eigenfunctions, reflecting the idea that an electron does not stay in the central region forever, as at one point it will tunnel through it into one of the leads. The lifetime of an electron in the center before it escapes into the lead α is goverened by a *rate operator* $\hat{\Gamma}_\alpha(\omega)$ [3]:

$$\hat{\Gamma}_\alpha(\omega) = \mathrm{i}\left[\hat{\Sigma}_\alpha^R(\omega) - \hat{\Sigma}_\alpha^A(\omega)\right]. \tag{2.12}$$

We may now obtain the expression for the transmission $\mathcal{T}_{\alpha\beta}$ from lead α to lead β as a trace over Green functions and rate operators [2, 3, 7]:

$$\mathcal{T}_{\alpha\beta}(\omega) = \mathrm{Tr}\left[\hat{\Gamma}_\alpha(\omega)\hat{G}^R(\omega)\hat{\Gamma}_\beta(\omega)\hat{G}^A(\omega)\right]. \tag{2.13}$$

Finally, we are able to obtain the current flowing across the central region. According to the assumptions of the Landauer-Büttiker approach, the population of electron energy states in each lead is independent of any other lead and may be described by a Fermi-Dirac distribution:

$$f_{\mathrm{FD}}(E; E_\mathrm{F}, T) = \left[\exp\left(\frac{E - E_\mathrm{F}}{k_\mathrm{B}T}\right) + 1\right]^{-1}. \tag{2.14}$$

The partial current $i_{\alpha\beta}$ induced in lead α due to the electron flow from lead β may then be calculated as follows [7]:

$$i_{\alpha\beta} = 2\int_\omega \mathrm{d}\omega\, \frac{1}{2\pi}\left[f_{\mathrm{FD}}(\omega - V_\alpha; \mu, T) - f_{\mathrm{FD}}(\omega - V_\beta; \mu, T)\right]\mathcal{T}_{\alpha\beta}(\omega), \tag{2.15}$$

where μ is the total chemical potential of the system and $V_{\alpha/\beta}$ are the respective bias voltage terms. The factor of two in front of this expression is due to the electron spin. We note that according to Eq. (2.15), backscattering current $i_{\alpha\alpha} = 0$, as when $\alpha = \beta$, the Fermi distributions in the two leads are identical. Thus, in order to compute backscattering current we would need to utilize a different expression. The total current I_α through lead α is the sum of partial currents that flow into that lead:

$$I_\alpha = \sum_{\beta \neq \alpha} i_{\alpha\beta}. \tag{2.16}$$

Conductance $\mathcal{G}_{\alpha\beta}$ is defined as a convolution of transmission with the thermal broadening function [3]:

$$\mathcal{G}_{\alpha\beta}(\omega) = \frac{2}{2\pi} \int \mathrm{d}\omega' \, \mathcal{T}_{\alpha\beta}(\omega') \frac{1}{4k_\mathrm{B}T} \mathrm{sech}^2 \left(\frac{\omega' - \omega}{2k_\mathrm{B}T} \right). \tag{2.17}$$

If $\left|\mu_\alpha - \mu_\beta\right| \ll k_\mathrm{B}T$, the conductance will be nearly constant, as the thermal broadening results in an integration over the entire energy space. Constant conductance means that the system is in the linear response regime. Conversely, when $\left|\mu_\alpha - \mu_\beta\right| \gg k_\mathrm{B}T$, thermal broadening acts like a Dirac delta function. This leads to linear proportionality between the conductance and the transmission:

$$\lim_{T \to 0} \mathcal{G}_{\alpha\beta}(\omega) = \frac{2}{2\pi} \mathcal{T}_{\alpha\beta}(\omega). \tag{2.18}$$

Hence, starting from the basic principles of the Landauer-Büttiker approach, we have derived the expressions for transmission, current and conductance.

3. TRANSPORT SOFTWARE AND SIMULATED SYSTEMS

In the preceding section, we have outlined a powerful theoretical framework for electronic transport in quantum systems. We note that the Landauer-Büttiker approach requires the solution of the Schrödinger equation for the central region and the leads before any transport properties may be computed. The Schrödinger equation can be solved analytically only for some specific cases e.g., harmonic oscillator, potential barrier, Hydrogen atom. Thus, we shift the emphasis in our study from analytically solvable systems to the ones that are solved approximately by computational means. We thus introduce TINIE (stands for **T**ransport **I**n **N**on-**I**nteracting **E**quilibrium), a versatile numerical framework that has been developed specifically to simulate transport phenomena in arbitrary two-dimensional transport systems. In the following sections, we shall outline the core algorithm behind the software and the key features. We will conclude this chapter by describing the transport systems that we will be analyzing in the following chapter.

3.1 Core algorithm

TINIE is a transport software package that has been written mostly in Python (version 3.6), but some of the optimized numerical routines have been written in C++, and wrapped into Python modules. Thus, we have combined the readability of a high-level language such as Python with the high-performance computing features of the lower-level language such as C++. TINIE is written with object-oriented programming, so all of the essential components of the code have been separated into different classes that would interact with each other throughout the simulation process. The algorithm is best described once there is a clear understanding of the way these classes are related to each other. These relations are summarized in Fig. 3.1.

First, we shall describe the object types and their essential functionality:

- `Center` object: represents the central region in the transport system. It is responsible for computing/retrieving the central region Hamiltonian $\hat{H}_C$ and the set of eigenfunctions of the central region $\{\psi_{C,j}\}$. These eigenfunctions are discretized and represented by `numpy` two-dimensional arrays, as we compute the eigenfunctions on a two-dimensional xy-grid with an adjustable grid spacing. The Hamiltonian is represented by a diagonal matrix. We note that such a representation is only possible if the eigenfunction set of the central region is orthonormal. Hence, orthonormality is a required condition for the proper code execution.

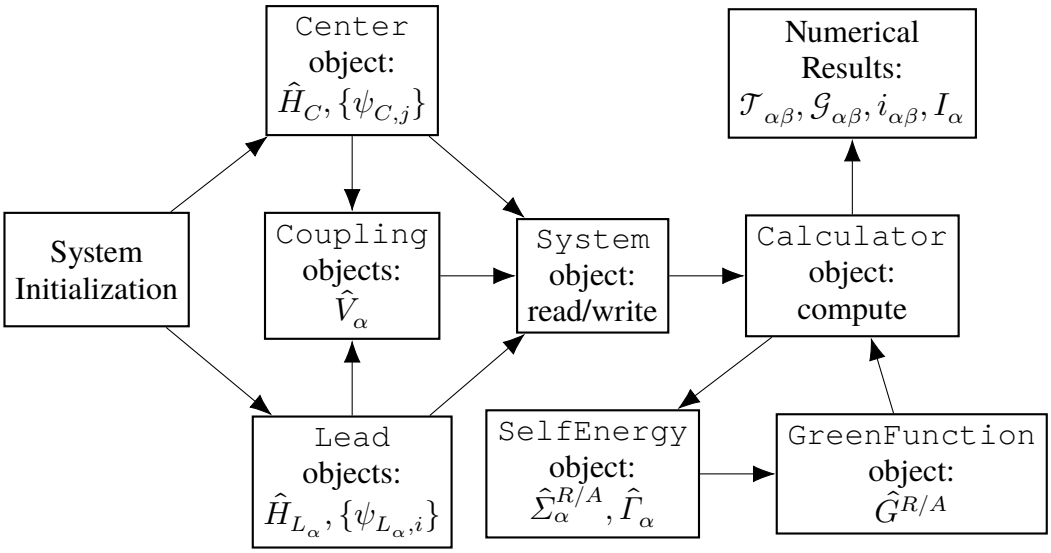

Figure 3.1. *TINIE object relation scheme.*

- `Lead` object: represents a particular lead region in the transport system. It is responsible for computing/retrieving the lead region Hamiltonian diagonal matrix $\hat{H}_{L_\alpha}$, as well as its set of eigenfunctions $\{\psi_{L_\alpha,i}\}$, discretized on the xy-grid. Similarly to the `Center` object, we assume orthonormality of the eigenstates.
- `Coupling` object: represents a coupling region between a particular lead and the central region. It is responsible for computing/retrieving the coupling $\hat{V}_\alpha$ between the central region and lead α, which is naturally represented by a `numpy` matrix array.
- `System` object: an interface that records the Hamiltonians and the coupling matrices in an hdf5-file via `h5py` module. As Hamiltonians and the coupling matrices do not change when we change the transport system parameters (such as the chemical potential or temperature), these files may then be reused for multiple transport calculations. Thus, `System` object also handles the retrieval of that data from an already existing file.
- `SelfEnergy` object: an interface that computes the self-energies $\hat{\Sigma}_\alpha^{R/A}$ and the rate operators $\hat{\Gamma}_\alpha$ for the transport system for varying values of probe energy ω.
- `GreenFunction` object: an interface that computes the Green functions $\hat{G}^{R/A}$ for the transport system for varying values of probe energy ω.
- `Calculator` object: interface that performs the main transport calculation of partial currents $i_{\alpha\beta}$, total currents I_α, transmission $\mathcal{T}_{\alpha\beta}$ and conductance $\mathcal{G}_{\alpha\beta}$.

Note that we have not described the functionality of those objects, mainly how the eigenfunctions, Hamiltonians or couplings are computed. The reason for that is simple: all of the above-mentioned objects are *abstract*, meaning that we can implement our own types of the central/lead/coupling region, specific to the transport system. This can be done by introducing a new class that inherits from one of those base classes and defining the respective methods for computation or retrieval of the system features.

Now we can outline the essential steps of the code execution:

Step 1: System initialization step. Initializes the `Center` object and the `Lead` objects.

Step 2: Coupling step. `Coupling` objects are initialized and the coupling matrices between the regions are computed and stored in those objects.

Step 3: System finalization step. `Center`, `Lead` and `Coupling` objects are passed into the `System` interface to store the transport system data. This completes the setup of the transport system, preparing it for the subsequent transport calculations.

Step 4: Transport initialization step. `System` object is passed into the `Calculator` object to retrieve the transport system data.

Step 5: Calculator initialization step. Within the `Calculator`, `SelfEnergy` object is initialized. It is then passed into the `GreenFunction` object for its initialization.

Step 6: Transport calculation step. The system transmission, conductance, and currents are evaluated at the user-defined values for chemical potential, temperature and lead biases using the self-energies, rate operators and Green functions as described in Sec. 2.3.

In essence, Steps 1-3 prepare the transport system for the calculation, while the transport calculation itself is performed during Steps 4-6. These two stages are thus completely independent from each other, as once the system is prepared and the system data stored in an hdf5-file, the transport calculations with that file can be performed at any convenient time with varying chemical potential values, temperatures, or lead biases. This completes the outline of the algorithm behind TINIE.

3.2 Features

Some of the features in TINIE might already be deduced from the way the code has been designed and the algorithm description of the previous section. Nonetheless, TINIE has more attributes that are worthy of mention. In this section, we shall discuss some of the core strengths that make TINIE a transport software with the potential to be developed further into a state-of-the-art simulation framework.

First and foremost, TINIE is extremely versatile. The abstract class approach to programming used in TINIE's design makes the code modular, allowing us to easily create new types of transport system objects and expand the code to be compatible with other software. For instance, currently, TINIE has a compatibility interface that allows it to interact with ITP2D [8], a numerical two-dimensional Schrödinger equation solver that uses an imaginary time propagation method to solve systems defined by arbitrary potentials. The wave functions and the Hamiltonian obtained through ITP2D can then be used in the initialization of the central region objects. Similarly, we can implement custom leads and custom coupling types, based on the corresponding abstract classes.

Secondly, TINIE performs its transport calculations from the *first principles*, that is, using the Landauer-Büttiker approach in its exact form, without any approximations besides those related to the wave function discretization and numerical differentiation/integration. One of TINIE's core strengths is its capability to perform calculations in a reasonable time without the need to resort to approximate theoretical transport formalisms. However, TINIE is also capable of utilizing some of the approximation regimes, such as the wide-band approximation regime, as will be demonstrated in the following sections.

Thirdly, TINIE has also been parallelized using `mpi4py` module. A lot of computations within the code are completely independent of each other. This has allowed us to parallelize the most computationally expensive parts of the code. Furthermore, as far as it has been tested, the performance speed increases linearly with the number of used processors. To that end, TINIE has been equipped with a parser user interface that easily allows us to perform numerical simulations in supercomputer clusters from the command line without any additional scripts. In particular, TINIE has been tested in the CSC Taito supercluster.

Last but not least, at this stage of development TINIE is compatible with systems in uniform and static magnetic fields perpendicular to the plane [9]. Other transport softwares e.g., KWANT [10], TRANSIESTA [11], SMEAGOL [12], OPENMX [13], NEXTNANO [14] do not provide such functionality to the extent of authors' knowledge. This feature of the code allows us to investigate a wider range of systems than ever before.

3.3 Simulated systems

To demonstrate the power of TINIE, we shall use the code to simulate transport phenomena in simple example systems. In the following subsections, we outline the physical description of those systems.

3.3.1 One-state system

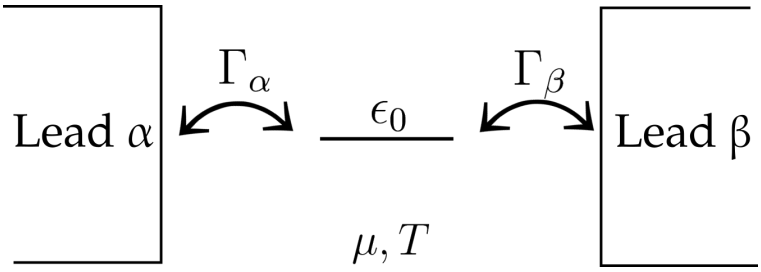

Figure 3.2. *Structure of a one-state transport system.*

We start with one of the simplest possible transport systems: a single energy state connected to two leads. Figure 3.2 shows the structure of such a system. In this system, we use the wide-band approximation regime. In particular, we assume that there are a lot of energy states below the Fermi energy. This assumption allows us to bypass the computation of the

coupling matrices. Instead, the coupling strength between the leads is specified by the rate operators. Thus, we need to know the following quantities to describe the transport system:

- Energy of the center region ϵ_0;
- Rate operators of the leads α and β: $\hat{\Gamma}_\alpha, \hat{\Gamma}_\beta$;
- Bias voltages in the leads V_α, V_β;
- Chemical potential μ;
- Temperature T.

It can be shown that in the case when the temperature is zero and the potential difference between the leads is small, we get the following expressions for the transmission and current [2]:

$$\mathcal{T}_{\alpha\beta} = \frac{2\pi}{2\left[V_\beta - V_\alpha\right]} I_\alpha \quad \text{and} \quad I_\alpha = \frac{\hat{\Gamma}_\alpha \hat{\Gamma}_\beta}{(\mu - \epsilon_0)^2 + \frac{(\hat{\Gamma}_\alpha + \hat{\Gamma}_\beta)^2}{4}}. \tag{3.1}$$

We benchmark the numerical precision of TINIE in computing the current and transmission for different values of the lead rate operators against these analytical results for zero temperature systems. At non-zero temperature we cannot obtain analytical closed-form expressions for neither the transmission nor the current. To test the performance of TINIE at non-zero temperatures we thus utilize Wolfram Mathematica software [15] to provide us with exact benchmark values.

3.3.2 Two-state system

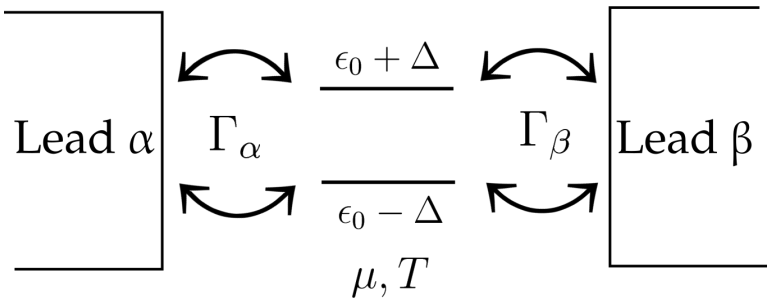

Figure 3.3. *Structure of a two-state transport system.*

We now move on to a more realistic two-state molecular junction connected to two leads. Figure 3.3 shows the structure of such a system. We consider a center region that can be interpreted as a molecule, e.g., benzene, where the lower energy state is the highest occupied molecular orbital (HOMO), while the higher energy state is the lowest unoccupied molecular orbital (LUMO). We construct the central region Hamiltonian of the form

$$\hat{H}_C = \begin{bmatrix} \epsilon_0 + \Delta & 0 \\ 0 & \epsilon_0 - \Delta \end{bmatrix},$$

where ϵ_0 is the Fermi energy and Δ is the parameter that we use to tune the energy spacing. Once again, we focus on the wide-band regime, where the rate operators of the leads are represented as matrices of the form [12]

$$\hat{\Gamma}_\alpha = \hat{\Gamma}_\beta = \begin{bmatrix} \Gamma & 0 \\ 0 & \Gamma \end{bmatrix},$$

where Γ is the coupling strength parameter to be adjusted.

3.3.3 Potential barrier system

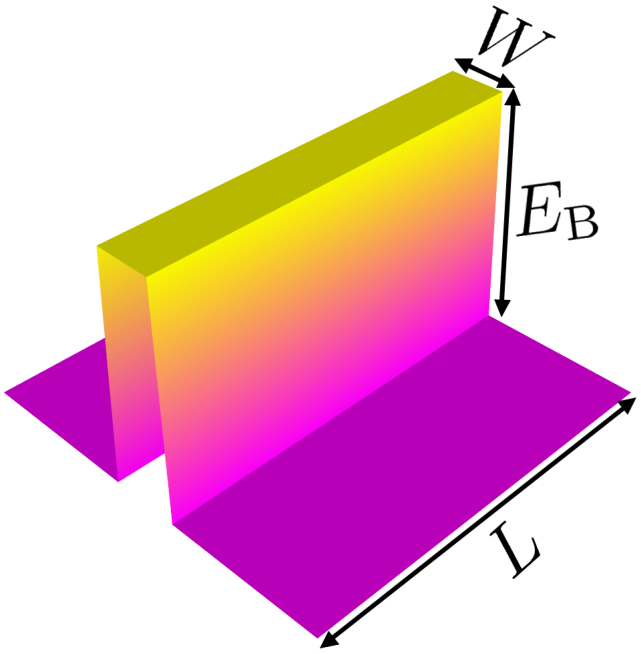

Figure 3.4. *Two-dimensional potential barrier system potential.*

We conclude with a conventional potential barrier system, which can be used to investigate electron tunneling properties in nanoscale systems. For this system, we utilize the Landauer-Büttiker approach. The potential of the central region can be written as

$$V_{\text{pot}}(x,y) = \begin{cases} E_{\text{B}} & x \in [-\frac{W}{2}, \frac{W}{2}] \wedge y \in [-\frac{L}{2}, \frac{L}{2}] \\ 0 & x \in (-\infty, -\frac{W}{2}) \cup (\frac{W}{2}, \infty) \wedge y \in [-\frac{L}{2}, \frac{L}{2}] \\ \infty & \text{elsewhere.} \end{cases} \tag{3.2}$$

Here E_{B} is the barrier height, L is the length of the central region in the y-direction and W is the width of the barrier in the x-direction. Figure 3.4 illustrates V_{pot} with its key parameters. The eigenfunctions of the central region in this potential are solved using ITP2D [8]. The central region is then connected to the system using the `Itp2dCenter` interface.

Two leads are connected to the central region. Specifically, the electrons are confined in the y-direction and are propagating in the x-direction. We use a harmonic oscillator potential in the y-direction and a standard particle-in-a-box potential in the x-direction. The eigenfunctions for the leads can be solved analytically, leading to [3]

$$\psi^L_{k,l}(x,y) = \mathcal{N}\cos\Big(k(x - x^L_{\max}) + \frac{\pi}{2}\Big)e^{-\frac{1}{2}y^2}H_l(y), \tag{3.3}$$

where $H_l(x)$ is the lth order Hermite polynomial and $\mathcal{N}$ is the normalization factor for the wave function. The indices l and k are the quantum numbers describing the system in x and y directions, respectively. The leads have been implemented in TINIE as `FiniteHarmonicLead` object.

Finally, we use the coupling of the form of Eq. (2.3), with the respective numerical integration routine implemented in TINIE as `OverlapCoupling` object. In particular, we investigate the behavior of conductance with varying values of the barrier energy E_{B}. Our setup mimics the schematics shown in Fig. 2.1.

4. RESULTS AND ANALYSIS

4.1 One-state system

For the one-state system introduced in Sec. 3.3.1, we set $\epsilon_0 = 500$, $\mu = 250$ in Eqs. (3.1). Additionally, we set the bias potentials of the two leads to be $V_\alpha = 0$ and $V_\beta = 1 \times 10^{-5}$. As the potential difference between the two leads is small, we compare our numerical results with the analytical result of Eq. (3.1). We set the lead rate operators $\hat{\Gamma}_\alpha = \hat{\Gamma}_\beta = \Gamma$ and compute the transmission and current in the system evaluated at various values of Γ. We start with the zero temperature case. Tables 4.1 and 4.2 show the results with the relative error estimates.

Table 4.1. *Comparison of the transmission values running through a zero-temperature one-state system computed using TINIE against the analytical values of Eq. (3.1). Relative error tolerances are near zero due to limitations of finite-precision arithmetics.*

Γ	Analytical $\mathcal{T}_{\alpha\beta}(\mu)$	TINIE $\mathcal{T}_{\alpha\beta}(\mu)$	Relative error
0.2	$6.3999959040 \times 10^{-7}$	$6.3999959040 \times 10^{-7}$	$\lesssim 10^{-15}$
0.4	$2.5599934464 \times 10^{-6}$	$2.5599934464 \times 10^{-6}$	$\lesssim 10^{-15}$
0.6	$5.7599668225 \times 10^{-6}$	$5.7599668225 \times 10^{-6}$	$\lesssim 10^{-15}$
0.8	$1.0239895143 \times 10^{-5}$	$1.0239895143 \times 10^{-5}$	$\lesssim 10^{-15}$
1.0	$1.5999744004 \times 10^{-5}$	$1.5999744004 \times 10^{-5}$	$\lesssim 10^{-15}$

Table 4.2. *Comparison of the current values running through a zero-temperature one-state system computed using TINIE against the analytical values of Eq. (3.1). The energy spacing for the numerical integration of Eq. (2.15) is set to* $\mathrm{d}\omega = 1 \times 10^{-7}$.

Γ	Analytical I_α	TINIE I_α	Relative error
0.2	$2.0371819677 \times 10^{-12}$	$2.0371819288 \times 10^{-12}$	1.910×10^{-8}
0.4	$8.1487122256 \times 10^{-12}$	$8.1487120699 \times 10^{-12}$	1.910×10^{-8}
0.6	$1.8334543837 \times 10^{-11}$	$1.8334543486 \times 10^{-11}$	1.910×10^{-8}
0.8	$3.2594598576 \times 10^{-11}$	$3.2594597953 \times 10^{-11}$	1.910×10^{-8}
1.0	$5.0928766929 \times 10^{-11}$	$5.0928765956 \times 10^{-11}$	1.910×10^{-8}

The results show that the values obtained numerically closely match the analytical values, especially in case of transmission, where the comparison yielded relative error estimates that were near zero due to the limitations of finite-precision arithmetics. For the current, the relative errors measurements can be detected, but they are very small. The errors arise from the numerical integration over transmission values in the region $\left[V_\alpha, V_\beta\right]$.

We note that both the transmission and the current increase with Γ. In the wide-band approximation regime, the value of Γ corresponds to the strength of the coupling of the lead to the central region. Hence, our results are plausible: the stronger the coupling, the higher the transmission.

In addition to the zero-temperature case, we have also investigated a non-zero temperature system with $k_{\mathrm{B}}T = 100$. We have changed bias potentials to $V_\alpha = 0$ and $V_\beta = 100$. The other system parameters are the same as before, and once again we let Γ vary. For such a system, there is no simple analytical result that we can use for comparison. Instead, we have used Wolfram Mathematica software to obtain numerically accurate benchmark results. We expect the current values to be higher in the non-zero temperature transport system due to the broader probe energy range, as well as the thermal broadening of the Fermi-Dirac energy distribution. The results of the calculations are summarized below in Table 4.3.

Table 4.3. *Comparison of the current values running through a non-zero temperature one-state system computed using TINIE against the values computed using Wolfram Mathematica. The energy spacing for the numerical integration of the current over the probe energies has been set to* $\mathrm{d}\omega = 0.01$.

Γ	Mathematica I_α	TINIE I_α	Relative error
0.2	$2.131426954 \times 10^{-2}$	$2.131426947 \times 10^{-2}$	2.824×10^{-9}
0.4	$4.263008442 \times 10^{-2}$	$4.263008417 \times 10^{-2}$	5.749×10^{-9}
0.6	$6.394736058 \times 10^{-2}$	$6.394736002 \times 10^{-2}$	8.702×10^{-9}
0.8	$8.526601433 \times 10^{-2}$	$8.526601334 \times 10^{-2}$	1.160×10^{-8}
1.0	$1.065859624 \times 10^{-1}$	$1.065859608 \times 10^{-1}$	1.484×10^{-8}

We observe that indeed the current values are much higher in case the temperature is non-zero, supporting our initial hypothesis.

4.2 Two-state system

To demonstrate how TINIE handles the two-state system described in Sec. 3.3.2, we compute the transmission of such a system, setting $\epsilon_0 = 0, \Delta = 1, \mu = 0$. Additionally, we set the lead bias voltages to $V_\alpha = -2, V_\beta = 2$. We consider this system in a zero-temperature environment. We then investigate the behavior of the system as we vary the coupling strength parameter Γ.

We expect to observe peaks in transmission at the eigenenergies of the center ($\epsilon_0 + \Delta = 1$ and $\epsilon_0 - \Delta = -1$), and we are interested in how those peaks vary with changing Γ. Figure 4.1 contains the results of the simulations.

As expected, we note the peaks in the transmission of the system at the eigenenergies of the central systems. When $\Gamma = 0$, the transmission is constantly zero, as in that case the leads are not coupled to the center at all. We can see that with increasing Γ the peaks get

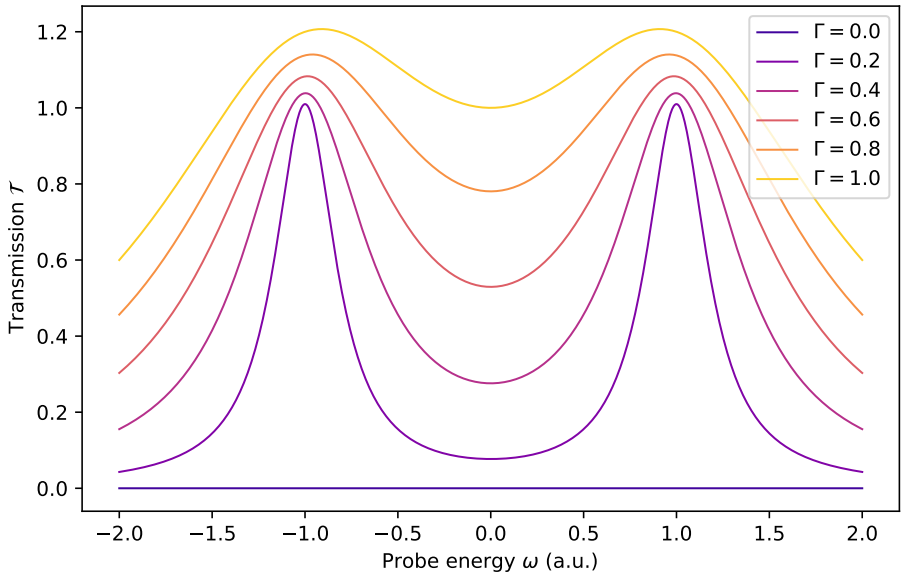

Figure 4.1. *Transmission in a two-state transport system with varying rate operator strengths.*

broader and higher, and tend to merge together as Γ goes to one. This result is plausible in view of the physical interpretation of Γ considered above. By increasing Γ, we increase the energy bandwidth of the electrons that may pass through the central region, leading to the widening of the transmission peaks around the eigenenergies. Hence, TINIE correctly captures the essential physical characteristics of the two-state system.

4.3 Potential barrier system

We conclude our numerical investigation by tackling a much more involved multi-state transport system using the full power of the Landauer-Büttiker approach. We consider two leads connected to the central region with a potential energy barrier [Eq. (3.2)]. The system has the following spatial confinements for the lead region and the center region:

- Center region: $x, y \in [-6, 6]$;
- Lead α: $x \in [-100, 0]$ and $y \in [-5, 5]$;
- Overlap α: $x \in [-6, 0]$ and $y \in [-5, 5]$;
- Lead β: $x \in [0, 100]$ and $y \in [-5, 5]$;
- Overlap β: $x \in [0, 6]$ and $y \in [-5, 5]$.

We set the width of the potential barrier to be 10, that is, $y \in [-5, 5]$. Additionally, we use the leads of the `FiniteHarmonicLead` variety (Sec. 3.3.3) and set the strength of the harmonic oscillator ω_0 to be one in both. We consider the behavior of conductance $\mathcal{G}$ from lead α to lead β, as we vary the barrier energy E_{B}. Furthermore, we investigate the temperature effects on the conductance. Intuitively, we expect the conductance to be low

when the probe electron energy is below the barrier energy. The conductance is expected to start increasing once the electron energy goes above the barrier. Figure 4.2 shows the results of the simulations.

In these numerical studies, we have considered the probe energy range $\omega \in [0, 15]$. In this energy range, each lead was found to contain 225000 eigenstates. As for the central region, solving its Schrödinger equation with ITP2D yields approximately 250 eigenstates in the same energy range. Consequently, this transport system is vastly more complicated than the simple systems we have discussed above. Nonetheless, all the obtained results seem physically plausible.

We note that in Fig. 4.2(a), the conductance only starts to grow and fluctuate when the energy of the probe electron surpasses that of the potential barrier. We observe similar behavior in Figs. 4.2(b) and 4.2(c). However, the picture is slightly more complex as demonstrated by the presence of minor conductance peaks below the barrier energy. They arise from the resonances in the system, as some of the central region eigenstates have eigenenergies below the energy of the potential barrier. The resonances occur when an eigenenergy of the lead closely matches one of the central region eigenenergies.

When the temperature of the system is close to zero, or small relative to the Fermi energy, every resonance results in a Dirac delta function-like peak in the conductance. As the temperature is increased to the scales comparable with the Fermi energy, these peaks become broader and smaller due to the effects of the thermal broadening on the conductance [Eq. (2.17)]. Thus, a single outlying conductance peak will get completely removed at high temperatures, while the peaks in the areas dense with conductance resonances will become more pronounced. This exact effect of temperature on conductance is observed in Fig. 4.2, further reassuring us that TINIE is capable of handling transport systems of high orders of complexity as well.

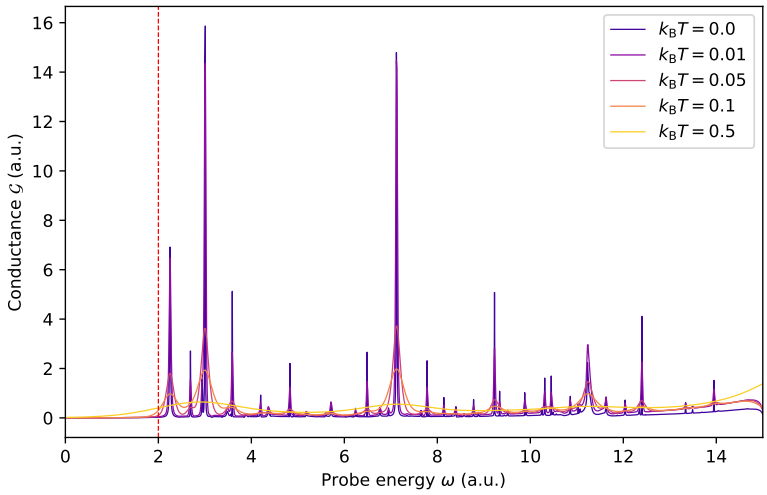

(a) Barrier energy $E_{\mathrm{B}} = 2$

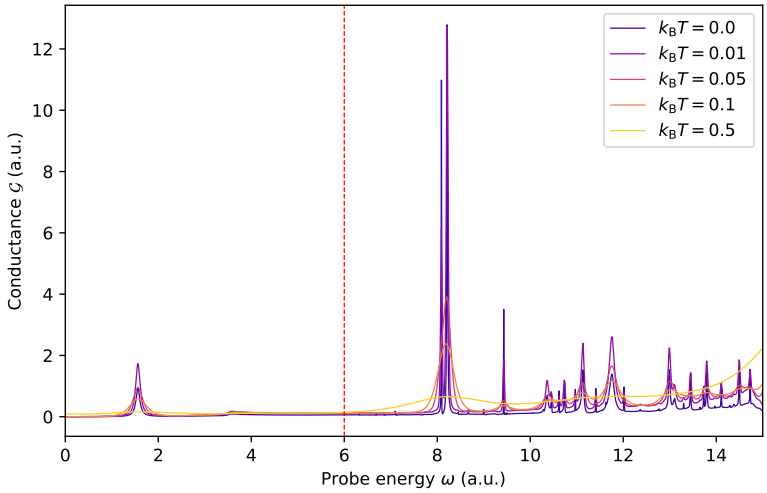

(b) Barrier energy $E_{\mathrm{B}} = 6$

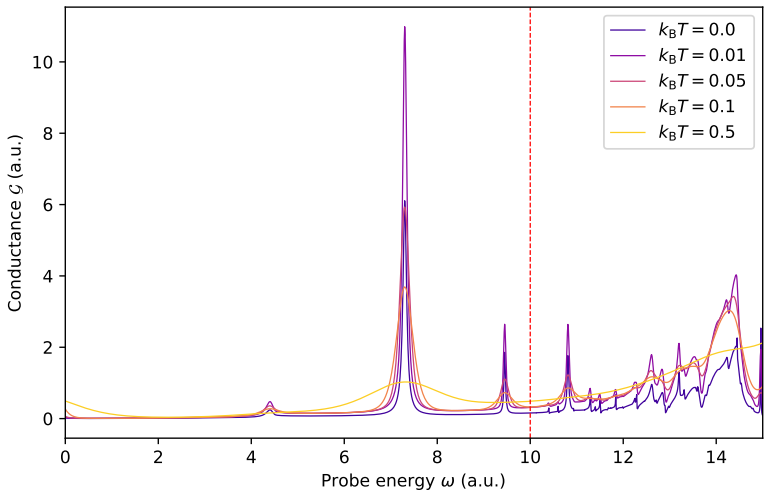

(c) Barrier energy $E_{\mathrm{B}} = 10$

Figure 4.2. *Conductance in the potential barrier system at varying system temperatures with* $\mu = 0.0, \eta = 0.02, V_\alpha = 0.0, V_\beta = 15.0$. *The conductance at zero temperature has been scaled by a factor of 50 to be visible on the figures.*

5. CONCLUSION

The field of quantum transport is rich with phenomena worthy of scientific investigation. In this thesis, we have merely scratched the surface of the field. Utilizing the basic principles of nanoscale transport that are encoded in the Landauer-Büttiker approach, we have developed TINIE, a versatile computational framework for simulation of electron transport in non-interacting equilibrium nanoscale systems.

In order to demonstrate functionality incorporated in TINIE, we have simulated three different multiple-lead transport systems: a single state molecular junction, a two-state molecular junction, and a potential barrier system. The numerical results obtained by simulating the single state molecular junction are in excellent agreement with the analytical results. We have found the behavior of transmission in the two-state molecular junction and conductance in the potential barrier system to match our initial hypotheses. This further reassures us of TINIE's validity as a transport code.

The main purpose of the thesis was to show the potential of TINIE as a tool to study transport in various systems. TINIE can be utilized to investigate systems in non-zero uniform magnetic fields, which is a feature that other transport codes to the extent of our knowledge do not possess. Under specific conditions, such transport systems exhibit some interesting properties. For instance, it has been shown in the prior studies that the presence of a magnetic field in the region confined to a potential that is randomly perturbed by impurities leads to the emergence of *quantum scars* [16]. Quantum scars are the regions of enhanced probability density in the quantum chaotic eigenstates, occurring around short unstable periodic orbits [17].

Systems with scarred eigenstates have been a topic of rising interest within the scientific community [18, 19, 20]. The implications *scarring* phenomena may have on the process of transport in a scarred system can be and will be studied in the future using TINIE. It is possible that scarred eigenstates lead to transmission peaks in the corresponding transport systems. By learning how to control the emergence of scars, we could potentially find a way to control the conductance properties of nanoscale devices. The study of scarring phenomena using TINIE could thus lead to many exciting and potentially ground-breaking discoveries.

REFERENCES

[1] M.M. Waldrop, More than moore, Nature, Vol. 530, Iss. 7589, 2016.

[2] M. Ventra, Electrical transport in nanoscale systems, Cambridge University Press, Cambridge, UK New York, 2008.

[3] S. Datta, Electronic transport in mesoscopic systems, Cambridge University Press, Cambridge, UK New York, 1997.

[4] P. Drude, Zur elektronentheorie der metalle, Annalen der Physik, Vol. 306, Iss. 3, 1900.

[5] R. Kubo, Statistical Physics II: Nonequilibrium Statistical Mechanics, Springer Berlin Heidelberg, Berlin, Heidelberg, 1991.

[6] L. Boltzmann, Weitere studien über das wärmegleichgewicht unter gasmolekülen, in: Kinetische Theorie II, Springer, 1970.

[7] G. Stefanucci, Nonequilibrium many-body theory of quantum systems: a modern introduction, Cambridge University Press, Cambridge, UK New York, 2013.

[8] P. Luukko, E. Räsänen, Imaginary time propagation code for large-scale two-dimensional eigenvalue problems in magnetic fields, Computer Physics Communications, Vol. 184, Iss. 3, 2013.

[9] H.U. Baranger, A.D. Stone, Electrical linear-response theory in an arbitrary magnetic field: A new fermi-surface formation, Physical Review B, Vol. 40, Iss. 12, 1989.

[10] C.W. Groth, M. Wimmer, A.R. Akhmerov, X. Waintal, Kwant: a software package for quantum transport, New Journal of Physics, Vol. 16, Iss. 6, 2014.

[11] M. Brandbyge, J.L. Mozos, P. Ordejón, J. Taylor, K. Stokbro, Density-functional method for nonequilibrium electron transport, Physical Review B, Vol. 65, Iss. 16, 2002.

[12] A.R. Rocha, V.M. García-Suárez, S. Bailey, C. Lambert, J. Ferrer, S. Sanvito, Spin and molecular electronics in atomically generated orbital landscapes, Physical Review B, Vol. 73, Iss. 8, 2006.

[13] T. Ozaki, K. Nishio, H. Kino, Efficient implementation of the nonequilibrium green function method for electronic transport calculations, Physical Review B, Vol. 81, Iss. 3, 2010.

[14] S. Birner, T. Zibold, T. Andlauer, T. Kubis, M. Sabathil, A. Trellakis, P. Vogl, Nextnano: general purpose 3-d simulations, IEEE Transactions on Electron Devices, Vol. 54, Iss. 9, 2007.

[15] W.R. Inc., Mathematica, Version 11.3. Champaign, IL, 2018.

[16] J. Keski-Rahkonen, P.J. Luukko, L. Kaplan, E. Heller, E. Räsänen, Controllable quantum scars in semiconductor quantum dots, Physical Review B, Vol. 96, Iss. 9, 2017.

[17] P.J. Luukko, B. Drury, A. Klales, L. Kaplan, E.J. Heller, E. Räsänen, Strong quantum scarring by local impurities, Scientific reports, Vol. 6, 2016.

[18] S. Sridhar, Experimental observation of scarred eigenfunctions of chaotic microwave cavities, Physical review letters, Vol. 67, Iss. 7, 1991.

[19] J. Stein, H.J. Stöckmann, Experimental determination of billiard wave functions, Physical review letters, Vol. 68, Iss. 19, 1992.

[20] T. Fromhold, P. Wilkinson, F. Sheard, L. Eaves, J. Miao, G. Edwards, Manifestations of classical chaos in the energy level spectrum of a quantum well, Physical review letters, Vol. 75, Iss. 6, 1995.